RESEARCH ARTICLE

Macromolecular Rapid Communications
www.mrc-journal.de

Hydrogel Rivet with Unidirectional Shape Morphing for Flexible Mechanical Assembly

April L. Ye, Haozhe Zhang, Baoyi Wu, Huanhuan Lu, Muqing Si, Kaihang Zhang, and Tao Chen**

Integrating diverse materials and functions into highly additive produce has piqued global interest due to the increasing demands of intelligent soft robotics. Nevertheless, existing assembly techniques, especially supramolecular assembly which heavily rely on precise chemical design and specific recognition, may prove inadequate when confronted with diverse external demands. Inspired by the traditional mechanical assembly, rivet connection, herein, a thermo-responsive hydrogel with unidirectional shape-morphing is fabricated and a stable mechanical assembly is constructed by emulating the rivet connection mechanism. This system employed poly(acrylamide-*co*-acrylic acid) [P(AAm-*co*-AAc)] to induce continuous swelling and hexylamine-modified polyvinyl alcohol (PVA-C6) as a molecular switch to control the swelling process. The hydrogel rivet, initially threaded through pre-fabricated hollows in two components. Subsequently, upon the disassociation of alkane chains the molecular switch would activate, inducing swelling and stable mechanical assembly via anchor structures. Moreover, to enhance the assembly strength, knots are introduced to enhance assembly strength, guiding localized stress release for programmed deformations. Additionally, the system can be remotely controlled using near-infrared light (NIR) by incorporating photo-thermal nanoparticles. This work presents a universal and efficient strategy for constructing stable mechanical assemblies without compromising overall softness, offering significant potential for the fabrication of integrated soft robots.

1. Introduction

Assembling components that vary in shape and materials, is essential for most high-value-added applications including deformable hydrogels, intelligent grippers, and soft robots, with complex 3D morphology and multi-function.[1–4] Whereas many strategies such as supramolecular assemble[5–8] and additive manufacturing[9–11] have been able to encode smart materials' biomimetic morphology and programmable deformation,[12–15] a significant gap between soft robotics and integrated rigid robotics still exits. For instance, utilizing supramolecular assemble to combine two stimuli-responsive hydrogels,[16–18] requires extensive efforts on the chemical design to strike a balance between the expected functionality and connection strength.[19–21] In contrast, traditional rigid robotics can easily integrate different functional components through simple mechanical assembly methods like screw connections and rivet connections.

Rivet connection, considered one of the mechanical assembly techniques, has long been regarded as a simple yet highly efficient strategy, making it indispensable in the manufacturing industry. As illustrated in **Scheme 1**a, a copper rivet can be inserted into two rigid components with prefabricated hollows by deforming its ends using an external hammer blow. Due to its unidirectional deformation, the copper rivet finds it challenging to return to its initial shape, ensuring stable connections under typical applications. However, this stability in rigid connections can lead to mechanical mismatches when applied in soft

A. L. Ye, H. Zhang
Ningbo Hanvos Kent School
Ningbo 315200, China
A. L. Ye
Georgia School Ningbo
Ningbo 315000, China
B. Wu, M. Si, T. Chen
Key Laboratory of Marine Materials and Related Technologies, Zhejiang Key Laboratory of Marine Materials and Protective Technologies, Ningbo Institute of Material Technology and Engineering
Chinese Academy of Sciences
Ningbo 315201, China
E-mail: wubaoyi@nimte.ac.cn; tao.chen@nimte.ac.cn
The ORCID identification number(s) for the author(s) of this article can be found under https://doi.org/10.1002/marc.202300586
B. Wu, M. Si, T. Chen
College of Material Chemistry and Chemical Engineering, Key Laboratory of Organosilicon Chemistry and Material Technology
Ministry of Education
Hangzhou Normal University
Hangzhou, Zhejiang 311121, China
H. Lu
College of Chemical Engineering
Ningbo Polytechnic
Ningbo 315800, China
K. Zhang
Department of Engineering Mechanics
Zhejiang University
Hangzhou 310027, China

DOI: 10.1002/marc.202300586

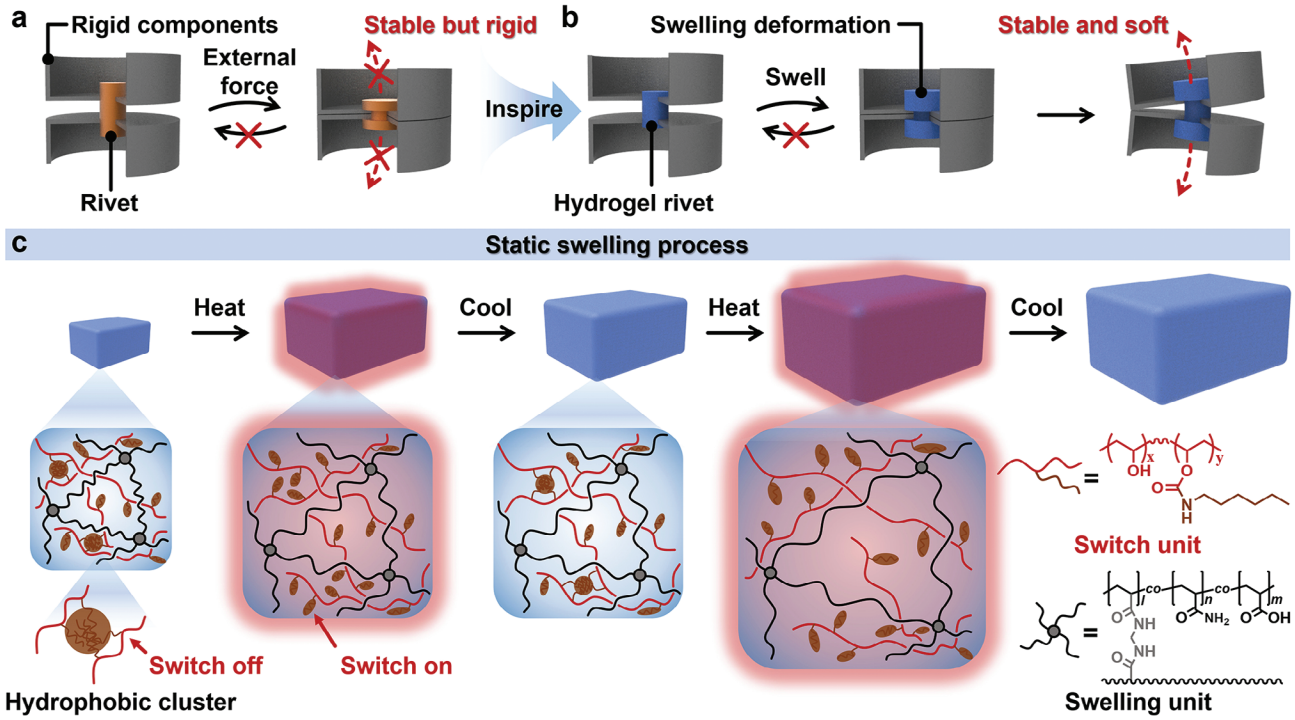

Scheme 1. The chemical design of hydrogel rivet with static swelling property. a) Schematic illustration showing the use of traditional copper rivets. b) Schematic illustration of the designed hydrogel rivets with their operation. c) Schematic illustration showing the chemical design of hydrogel rivet with static swelling property. The PVA-C6 is utilized as a molecular switch to control the deformation process via the thermo-responsive hydrophobic clusters.

mechanical assemblies.[22–24] Thus, drawing inspiration from the above assembly mechanism, employing a deformable hydrogel as a rivet, and altering its initial shape through a shape-morphing process before inserting it into the components to create a stable connection, would be a considerable solution for the soft mechanical assembly (Scheme 1b).[25–28]

Upon the aforementioned mechanism, the unidirectional self-deformable property is the key element in the chemical design of hydrogel rivets. To overview the existing deformable hydrogel, there are two major classifies of deformable hydrogels: hydrogel actuators and shape memory hydrogels.[29–31] According to our previous works, hydrogel actuators typically exhibit reversible deformation via stimuli-responsive swelling and deswelling,[32–34] so using them as hydrogel rivets might not be able to generate a stable connection. Similarly, shape memory hydrogel could not deform from a simple bar shape to a complex riveted shape.[35–38] In fact, hydrophilicity-induced self-swelling of hydrogel in a water environment, is the ideal unidirectional shape morphing process, which has often been overlooked due to the emphasis on controlling the swelling process.[39–41] Existing works invariably pay more attention to how to counteract the swelling process or directly utilize swelling-equilibrium hydrogel in hydrogel research.[42–45] Therefore, utilizing the hydrogel actuator as a swelling source while applying the shape memory process as the control unit,[46–48] would be a challenging but feasible solution to statically control the swelling process of hydrogel and further realize the application of hydrogel rivet for soft mechanical assembly.

Herein, we constructed a thermo-responsive hydrogel rivet with the static swelling property where poly(acrylamide-*co*-acrylic acid) [P(AAm-*co*-AAc)] was severed as swelling source and hexylamine-modified polyvinyl alcohol (PVA-C6) was utilized as a molecular switch to continuously control the swelling situation. Owing to the hydrophobicity of alkane chains, the hydrophobic cluster could be generated in a hydrogel rivet and acted as a temporary cross-linker to impede the chain elastic-induced swelling of the P(AAm-*co*-AAc) network, suspending the swelling process. Notably, this molecular switch could also be turned on in response to external temperature. As the temperature increased, the hydrophobic cluster would gradually disassociate, releasing the network restriction and allowing the swelling process to resume (Scheme 1c). Different from existing thermo-responsive hydrogel actuators, the thermo-responsiveness of the hydrophobic clusters does not alter the hydrophilicity of the network during heat-cool cycles. Consequently, this deformation process remains unidirectional and relies entirely on the swelling behavior of the P(AAm-*co*-AAc) network.

To enhance the deformability of the hydrogel rivet, we incorporated knots into the surface of the PVA-C6/P(AAm-*co*-AAc) hydrogel, enabling programmed deformation. Furthermore, by introducing photothermal nanoparticles, specifically Fe_3O_4, this hydrogel could be endowed with photo-thermal properties, allowing remote control through near-infrared light (NIR). Leveraging the aforementioned unidirectional deformability and control strategy, the PVA-C6/P(AAm-*co*-AAc) hydrogel can serve as a hydrogel rivet, forming stable connections between two rigid components via a thermo-induced swelling process. Moreover, due to the soft and wet characteristics of the hydrogel, the assembled components can exhibit soft deformations such as stretching and bending. As a result, hydrogel rivets have remarkable

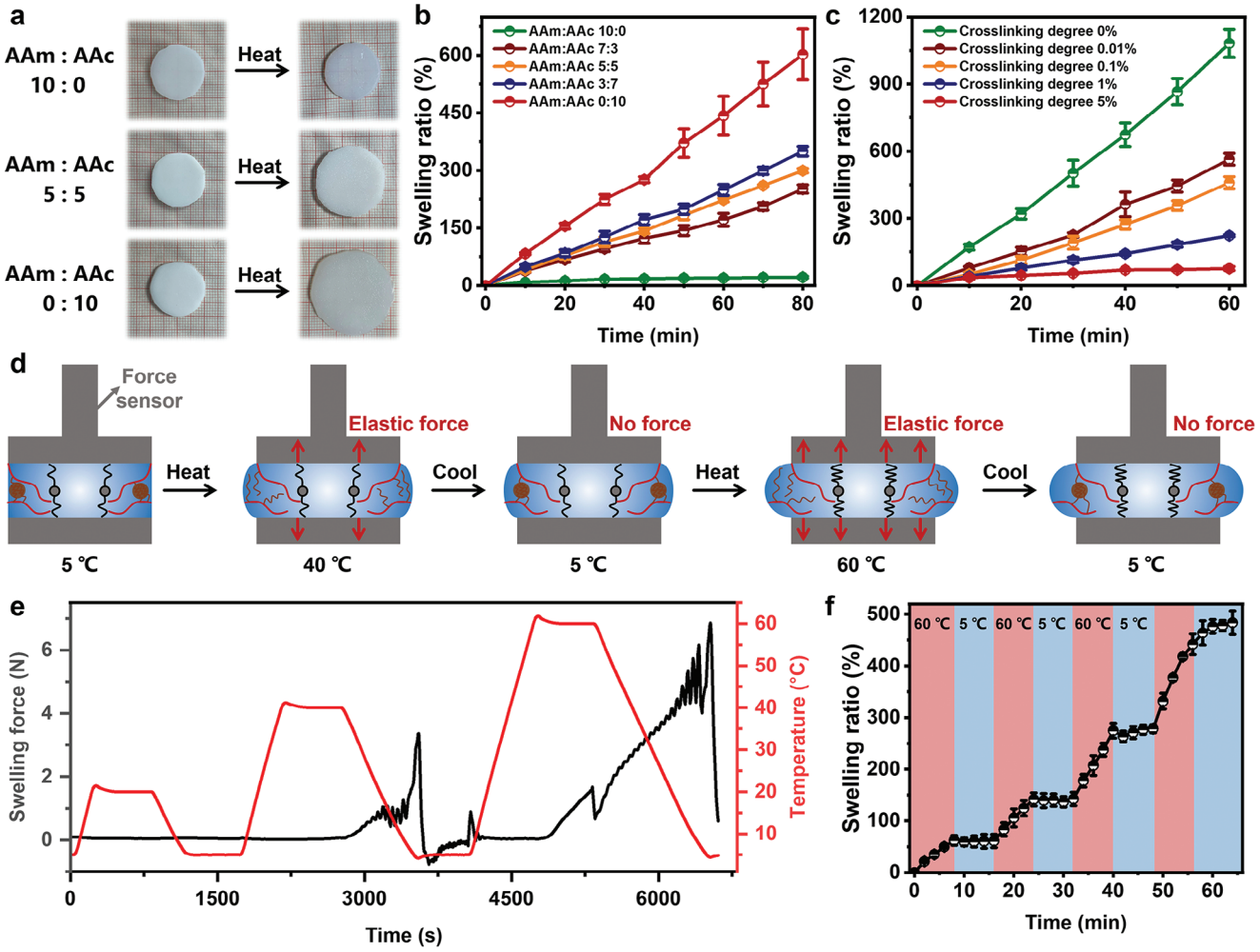

Figure 1. Swelling properties and swelling control of PVA-C6/P(AAm-*co*-AAc) hydrogel. a) Images showing different proportions of AAm and AAc resulted in different swelling volumes over a certain period of time. b) Quantitative analysis of PVA-C6/P(AAm-*co*-AAc) hydrogel different swelling ratios under the conditions of different AAm and AAc ratios. c) Quantitative analysis of PVA-C6/P(AAm-*co*-AAc) hydrogel different swelling ratios under the conditions of different crosslinking degrees. d) Schematic illustration of the elastic force of PVA-C6/P(AAm-*co*-AAc) hydrogel released outward at different temperatures. e) The swelling force of the PVA-C6/P(AAm-*co*-AAc) hydrogel related to the ambient temperature. f) Quantitative analysis of the dynamic multi-stable shapes of the PVA-C6/P(AAm-*co*-AAc) hydrogel strip during the swelling deformation process.

advantages compared to traditional rivets. The soft nature of hydrogel rivets allows them to easily accomplish bending deformations, making them highly versatile for connecting different soft components, and avoiding them from damaging the soft components. Additionally, the controllable thermo-responsive swelling allows for the assembly of PVA-C6/P(AAm-*co*-AAc) hydrogel, which is more convenient and efficient compared to traditional rivet connections. Thus, we believe that this work provides valuable insights into the application of deformable hydrogels in soft mechanical assembly and the field of soft robotics.

2. Result and Discussion

2.1. Swelling-Induced Static Shape Morphing Process

To statically control the shape morphing process, alkyl chains (hexylamine) were attached to the hydrophilic backbone, PVA. Due to the hydrophobicity of alkyl chains, the modified PVA could generate hydrophobic clusters in cool water and disassociate in hot water. It is important to note that while long alkane chains can also facilitate reversible cluster aggregation, they are unsuitable for use in a hydrogel system due to excessive hydrophobicity.[49,50] As previously discussed, to generate deformation, the product was incorporated into a hydrophilic hydrogel network to fabricate a double network hydrogel, referred to as the PVA-C6/P(AAm-*co*-AAc) hydrogel. In this structure, the hydrophilic hydrogel network serves as the source of swelling, while the PVA-C6 network acts as a molecular switch to control the swelling process. As depicted in **Figure 1**a, when polyacrylamide (PAAm) was employed as the hydrophilic network, the PVA-C6/P(AAm-*co*-AAc) hydrogel only achieved a 20% increase in size when exposed to hot water, which may not be sufficient to generate significant deformation. To enhance the deformability, acrylic acid monomers were copolymerized with acrylamide, constructing the P(AAm-*co*-AAc) network. Owing to the

polyelectrolyte effect of PAAc, with the increase in the proportion of AAc to AAm, the swelling ratio of PVA-C6/P(AAm-*co*-AAc) hydrogel would further increase (Figure 1b). Besides, covalent crosslinking interaction which was generated by *N*,*N*′-methylene bis(acrylamide) (BIS), could also influence the swelling ability. Typically, the addition of a crosslinker reduces the polymer chain length between crosslinking points in the 3D network, limiting chain flexibility and resulting in reduced swelling properties (Figure 1c). Notably, there was another crosslinking interaction: a thermos-responsive cluster of the PVA-C6 network, which played an essential role in the swelling process. The hydrophobic clusters formed by short alkyl side chains would disassociate in high temperatures, breaking physical crosslinking interactions and releasing the swelling ability of the P(AAm-*co*-AAc) network in hot water. On the other hand, the hydrophobic clusters would aggregate under cold water condition. Thus, higher temperatures in certain ranges would lead to more hydrophobic clusters disassociating, facilitating the swelling process (Figure S1, Supporting Information). In a word, the swelling property of PVA-C6/P(AAm-*co*-AAc) hydrogel could be regulated by changing the composition of the hydrogel and environmental temperature according to different application requirements.

The thermo-responsive hydrophobic clusters within the PVA-C6/P(AAm-*co*-AAc) hydrogel serve a dual role, functioning not only as controllers of its swelling behavior but also as molecular switches orchestrating the swelling process. For example, as shown in Figure 1d, the PVA-C6/P(AAm-*co*-AAc) hydrogel was placed inside a parallel fixture with a fixed pitch in an aqueous environment. As the temperature gradually increased to 20 °C, a portion of the hydrophobic clusters dissociated, while the majority persisted, acting like "tightropes" restraining the elasticity of the P(AAm-*co*-AAc) chains. Subsequently, upon heating the water to 40 °C, an increasing number of hydrophobic clusters disassociated, reinitiating the swelling process of the PVA-C6/P(AAm-*co*-AAc) hydrogel. Thus, chain-elastic-induced forces were generated and aggregated on the surface of hydrogel, which could be meticulously monitored by a highly sensitive sensor. Interestingly, when the environment cooled back to 5 °C, short alkyl side chains rapidly regenerated, reestablishing hydrophobic clusters within the P(AAm-*co*-AAc) network. Therefore, the force sensor reading returned to zero, signifying complete restriction of the chain elasticity within the P(AAm-*co*-AAc) network by the PVA-C6 network. Moreover, when the environment was heated to a higher temperature like 60 °C, the PVA-C6/P(AAm-*co*-AAc) hydrogel would generate significantly greater elastic forces due to the higher swelling ratio. It is worth noting that a slight delay occurred between the temperature increase and the evident rise in swelling force, as the PVA-C6/P(AAm-*co*-AAc) hydrogel required some time to reach full swelling potential. In addition, the reversible generation of hydrophobic clusters could also be evaluated by rheological properties. In a 60 °C water environment, the loss modulus exceeded the storage modulus, while in a 5 °C water environment, the storage modulus consistently surpassed the loss modulus. Additionally, the storage modulus would increase from 5×10^3 to 5×10^5 with the temperature decreased from 60 to 5 °C, which indicated that hydrogel remained tough at the lower temperature but became softer at higher temperature with disassociation of hydrophobic clusters (Figure S2, Supporting Information).

The effectiveness of the PVA-C6 network as a molecular switch is further corroborated by its swelling ratio, denoting the percentage change in mass. As shown in Figure S3, Supporting Information, when the PVA-C6/P(AAm-*co*-AAc) hydrogel was immersed in 60 °C water, it swelled by 70% of its initial mass within 8 min, driven by the hydrophilicity of the P(AAm-*co*-AAc) network. Subsequently, the hydrogel was rapidly transferred to a 5 °C water bath, triggering the aggregation of hydrophobic clusters and suspending the swelling process. Consequently, the mass of the PVA-C6/P(AAm-*co*-AAc) hydrogel exhibited negligible further growth during the remaining duration. Notably, as the PVA-C6/P(AAm-*co*-AAc) hydrogel swelled, the concentration of molecular switch would decrease, which weakened the restriction effect of hydrophobic clusters, causing the uncontrollable swelling process of the P(AAm-*co*-AAc) network in 5 °C water. In fact, owing to the noteworthy thermo-responsiveness of PVA-C6 network, the PVA-C6/P(AAm-*co*-AAc) hydrogel could efficiently control the swelling process within a 600% swelling ratio. Therefore, when being alternatively immersed in different temperatures, the PVA-C6/P(AAm-*co*-AAc) hydrogel would swell in 60 °C water while remaining stable in 5 °C water, which proved that the thermo-responsive hydrophobic clusters could act as an effective and timely molecular switch for the swelling process of the PVA-C6/P(AAm-*co*-AAc) hydrogel, allowing it to stop and remain stable in any stage of swelling (Figure 1f). This outstanding multi-static shape morphing in PVA-C6/P(AAm-*co*-AAc) hydrogel's swelling process inspired us to further expand its application and function.

2.2. Restricting-Domain Induced Multi-Dimensional Deformation of PVA-C6/P(AAm-*co*-AAc) Hydrogel

Although PVA-C6/P(AAm-*co*-AAc) hydrogel has been capable of generating static deformation by controlling the swelling process, it could only exhibit simple volume change due to the isotropic structure. Recently, scientists have turned their attention to encoding hydrogels with anisotropic structures to imbue them with programmable deformation capabilities. In this study, we introduce a novel approach by incorporating knots into the surface of the hydrogel, inducing isotropic hydrogels to exhibit programmed deformations. As illustrated in **Figure 2**a, a length of cotton cord was threaded through the ends of the PVA-C6/P(AAm-*co*-AAc) hydrogel and securely knotted at both ends. When this hydrogel was immersed in 60 °C water, the presence of the cotton cord restricted its horizontal swelling. Consequently, the swelling stresses were channeled into the vertical direction, leading to the hydrogel undergoing a transformation from a 1D strip shape to a 2D curved shape. To quantitatively evaluate the deformation ratio, the characteristic shape parameter (RSP) which was defined as the ratio between the height and width of the folded shape, was applied. Furthermore, to enhance our understanding of the restricting-domain-induced shape deformation process, we conduct finite element modeling, which yields results highly consistent with our experimental findings (Movie S1, Supporting Information). Benefiting from the static swelling property of PVA-C6/P(AAm-*co*-AAc) hydrogel, the transient shape of composite hydrogel could be quickly fixed during the thermo-responsive deformation process, which means

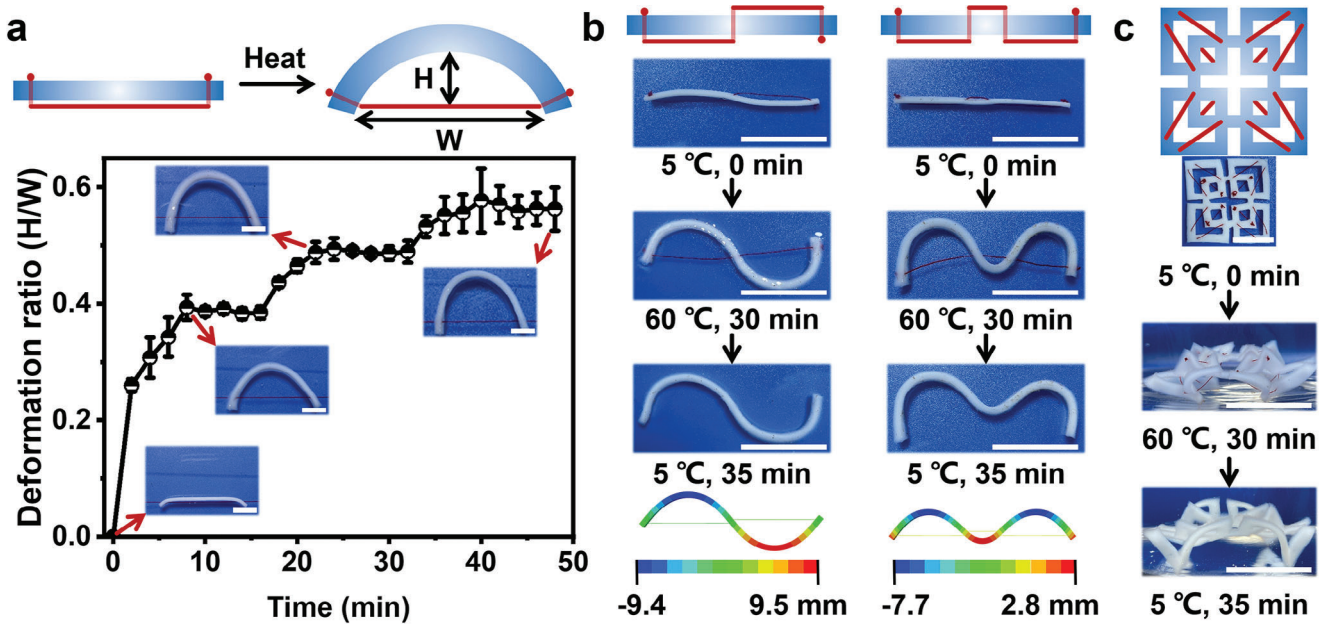

Figure 2. Restricting-domain induced multi-dimensional deformation of PVA-C6/P(AAm-*co*-AAc) hydrogel. a) Quantitative analysis of the restricting-domain induced multi-stable deformation of PVA-C6/P(AAm-*co*-AAc) hydrogel strip during the swelling process. b) Schematic illustration and images showing 2D restricting-domain induced complex deformations of PVA-C6/P(AAm-*co*-AAc) hydrogel and its mechanical models. c) 3D restricting-domain induced complex deformation of PVA-C6/P(AAm-*co*-AAc) hydrogel. Scale bars: 2 cm.

the deformation ratio could be regulated by controlling the generation of hydrophobic clusters. Based on this strategy, we further demonstrated the 2D complex deformation. As shown in Figure 2b, through encoding the situation of knots, a simple hydrogel strip could exhibit "S" and "M" shape complex deformation, respectively (Movie S2, Supporting Information). Moreover, if this strategy is applied to a hydrogel sheet, the 2D origami-shaped hydrogel could further generate a more complex 3D shape. Notably, the hydrophobic clusters not only suspend the deformation process but also fix the shape at a specific temperature. Therefore, even after the removal of the cotton cord, the PVA-C6/P(AAm-*co*-AAc) hydrogel retains its complex morphologies (Figure 2c).

Incorporating knots not only imparts anisotropic deformation capabilities to isotropic hydrogels but also introduces innovative deformation modes, such as delayed deformation (**Figure 3**a). For instance, as shown in Figure 3b, various lengths of cotton cord were affixed to hydrogel strips of identical initial lengths and subsequently immersed in 60 °C water (Movie S3, Supporting Information). Because the attached length was longer than the initial hydrogel strip, the hydrogel strip initially underwent isotropic deformation until the cord became taut. Then, limited by the cotton cord, the deformation mode would transfer to isotropic bending deformation (Figure S5, Supporting Information). Thus, by selecting the initial length of the cotton cord, the onset time of anisotropic deformation could be encoded into different parts of the hydrogel strip, generating time-dependent complex deformation (Figure S6, Supporting Information). As demonstrated in Figure 3c, the left segment of the hydrogel strip underwent deformation first, followed by the middle segment, and finally, the right segment, resulting in a gradual time-dependent isotropic deformation (Movie S4, Supporting Information). Similar to the previous discussion, all shapes produced by this strategy could be maintained in the 5 °C water when the restriction was removed (Figure 3d).

2.3. Light-Steered Complex Deformation and Remote Control

Furthermore, to enhance the operability of the above system, some photo-thermal particle (Fe_3O_4) was added into the hydrogel precursor in the manufacturing process, fabricating PVA-C6/P(AAm-*co*-AAc) photo-thermal hydrogel. Owing to the photo-thermal effect of Fe_3O_4, the surface temperature of PVA-C6/P(AAm-*co*-AAc) photo-thermal hydrogel experienced rapid elevation upon exposure to NIR light (**Figure 4**a). As a result of Figure 4b, when 4 W NIR light was applied, the surface temperature of PVA-C6/P(AAm-*co*-AAc) photo-thermal hydrogel would increase to 60 °C in 3 min. Additionally, the highest temperature could also be regulated by adjusting the NIR source. Upon this efficient photo-thermal effect, all of the aforementioned deformation modes could be replicated and operated remotely. As demonstrated in Figure 4c, when 4 W NIR light irradiated onto the surface of PVA-C6/P(AAm-*co*-AAc) photo-thermal hydrogel in 5 °C water, the hydrogel temperature would quickly increase, which induced the disassociation of hydrophobic cluster of PVA-C6 network and restarted the swelling process. Consequently, the mass of the hydrogel increased to 260% of its initial mass within 30 min. Similarly, when employing the restricting-domain strategy, the hydrogel could achieve anisotropic deformation under remote control, with the deformation ratio reaching 0.42 within 30 min (Figure S7, Supporting Information).

Moreover, the application of the photo-thermal effect not only confers remote controllability over the deformation of the

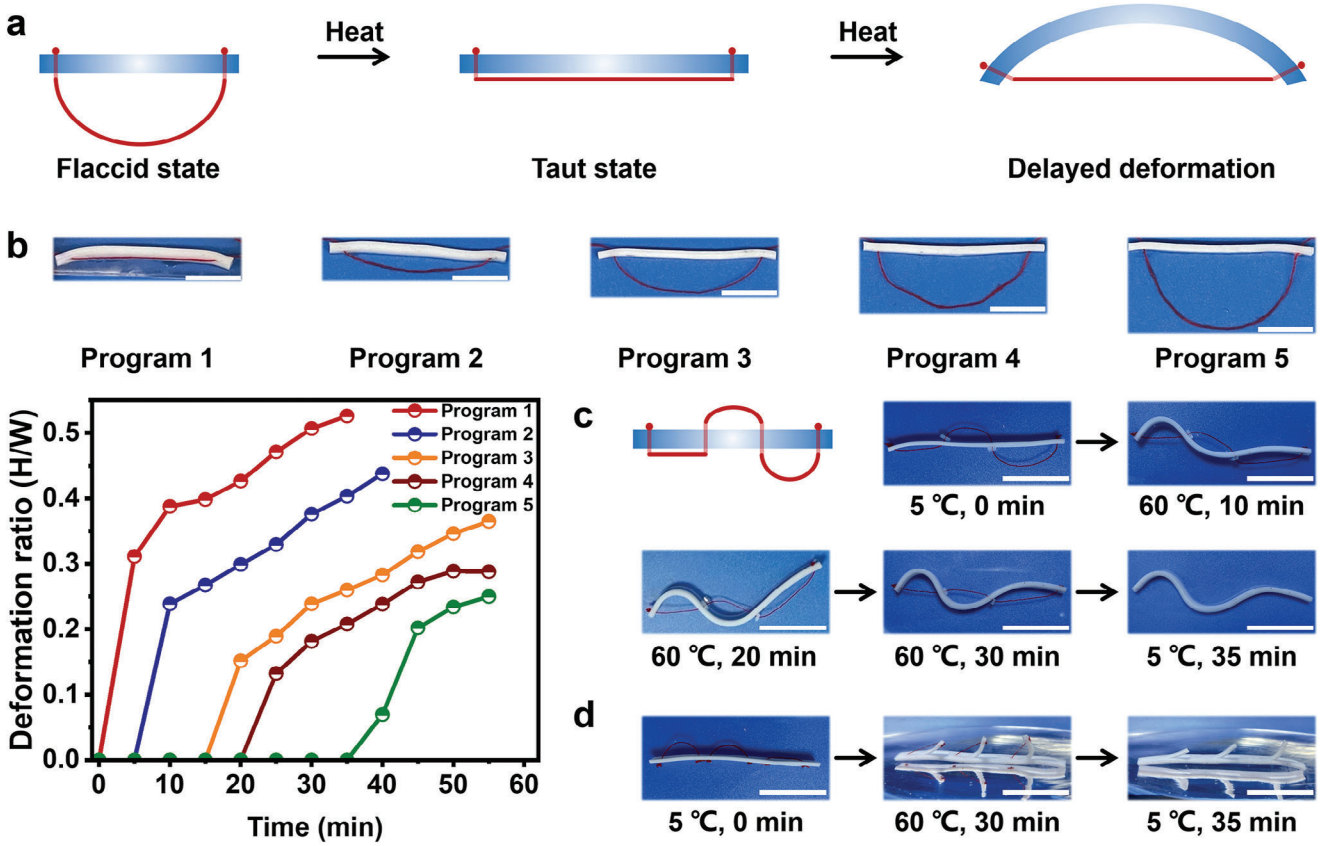

Figure 3. Delayed restricting-domain induced complex deformation in PVA-C6/P(AAm-*co*-AAc) hydrogel. a) Illustration showing the mechanism of delayed deformation in PVA-C6/P(AAm-*co*-AAc) hydrogel. b) The aspect ratio of PVA-C6/P(AAm-*co*-AAc) hydrogel with the same initial length but different restricting-domain lengths over time. c) Images showing 2D postponed-restricting-domain induced complex deformation of PVA-C6/P(AAm-*co*-AAc) hydrogel with different initial restricting lengths over time. d) Images showing 3D postponed-restricting-domain induced complex deformation of PVA-C6/P(AAm-*co*-AAc) hydrogel. Scale bar: 1 cm.

PVA-C6/P(AAm-*co*-AAc) hydrogel but also allows for the precise encoding of heat distribution, enabling the programming of surface morphologies. As demonstrated in Figure S8, Supporting Information, when 4 W NIR light was directed at the central region of a hydrogel sheet, only the temperature of the circular focal area increased, triggering isotropic swelling. Thus, limited by the surrounding non-deformable region, the excess selling stress had to be released to the vertical direction, generating the 3D bulge shape. Similarly, with the assistance of a photo-mask, a heart-shaped pattern could be printed onto the surface of PVA-C6/P(AAm-*co*-AAc) photo-thermal hydrogel, causing the 3D heart-shaped bulge after the swelling process (Figure S9, Supporting Information). Notably, various patterns such as "S," "T," "A," "R" could be printed in the same way, yielding corresponding 3D letter formations (Figure 4d). Intriguingly, this light-steered strategy could further endow hydrogel with a multilevel structure. For example, a larger circle area on the hydrogel sheet was irradiated for 15 min first, generating a 3D convex shape. Subsequently, a smaller circle area on the topper of the 3D convex shape was irradiated by NIR light. Thus, the topper area of the hydrogel sheet would further swell, exhibiting a multilevel 3D bulge shape (Figure 4e).

2.4. Applications for Soft Mechanical Assembly

Drawing inspiration from rivet connections, the concept of applying the PVA-C6/P(AAm-*co*-AAc) hydrogel with unidirectional shape morphing to the field of rivets resulted in the application of soft mechanical assembly. To demonstrate the soft mechanical assembly, two rigid mold components with pre-fabricated hollows were prepared (**Figure 5**a). Subsequently, a cylindrical hydrogel rivet with an identical diameter was precisely inserted into the hollows of the two rigid components. The composite assembly was then fully immersed in 60 °C water for 1.5 h, allowing the ends of the hydrogel rivet to swell until its diameter surpassed that of the component holes completely. This process resulted in the creation of a stable assembly capable of supporting a 55 g weight load (Figure 5b). Notably, with the disassociation of hydrophobic clusters, the PVA-C6/P(AAm-*co*-AAc) hydrogel would become softer. Thus, when a rotunda mold was covered at the end of the hydrogel rivet, the cylindrical hydrogel would gradually fill up the rotunda cavity and be reshaped as a rotunda shape (Figure S10, Supporting Information). In comparison to existing hydrogel actuators, the PVA-C6/P(AAm-*co*-AAc) hydrogel offers a more stable connection due to its unidirectional shape

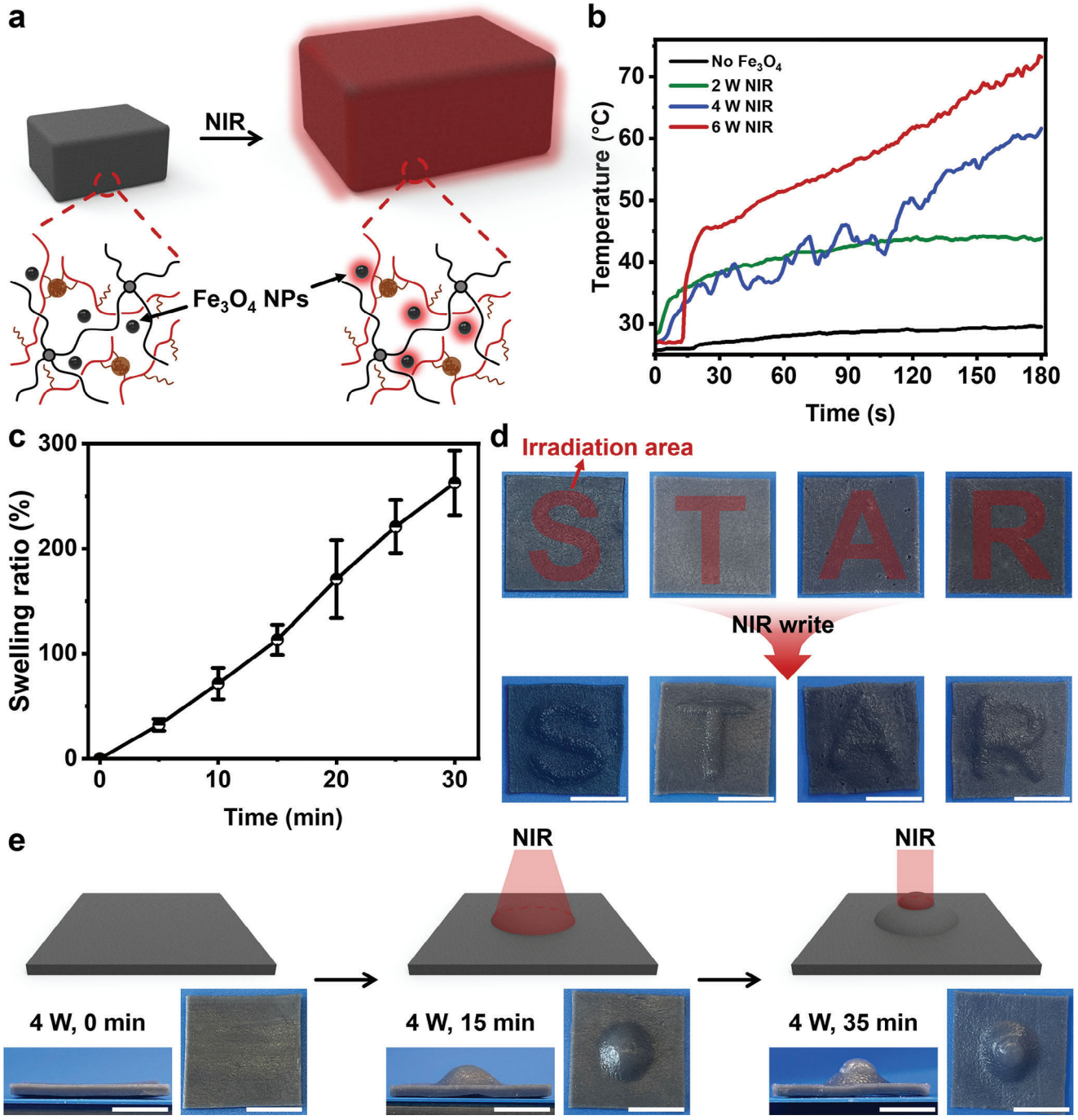

Figure 4. Light-steered complex deformation of PVA-C6/P(AAm-*co*-AAc) photo-thermal hydrogel. a) Schematic illustration showing the operation of photo-thermal effect in the PVA-C6/P(AAm-*co*-AAc) hydrogel under NIR irradiation. b) The photo-thermal effect of PVA-C6/P(AAm-*co*-AAc) hydrogel under NIR light with different export power. c) Quantitative analysis of the swelling ratio of PVA-C6/P(AAm-*co*-AAc) photo-thermal hydrogel over time. d) NIR wrote the word "STAR" on the hydrogel by using remote-controlled restricting-domain swelling. e) Superposition of double circle morphology of PVA-C6/P(AAm-*co*-AAc) photo-thermal hydrogel. Scale bars: 1 cm.

morphing. For example, as shown in Figure S11, Supporting Information, when the Poly(*N*-isopropyl acrylamide) (PNIPAm) was utilized as a hydrogel rivet to assemble the same rigid components, it could securely grip components in low temperature owing to the swelled shape. However, as the external temperature exceeded the lower critical solution temperature (LCST) of PNIPAm, the hydrogel rivets shrank, compromising the stability of the connection. On the contrary, regardless of the temperature changes, the PVA-C6/P(AAm-*co*-AAc) hydrogel can only deform in the swelling direction, ensuring a more dependable

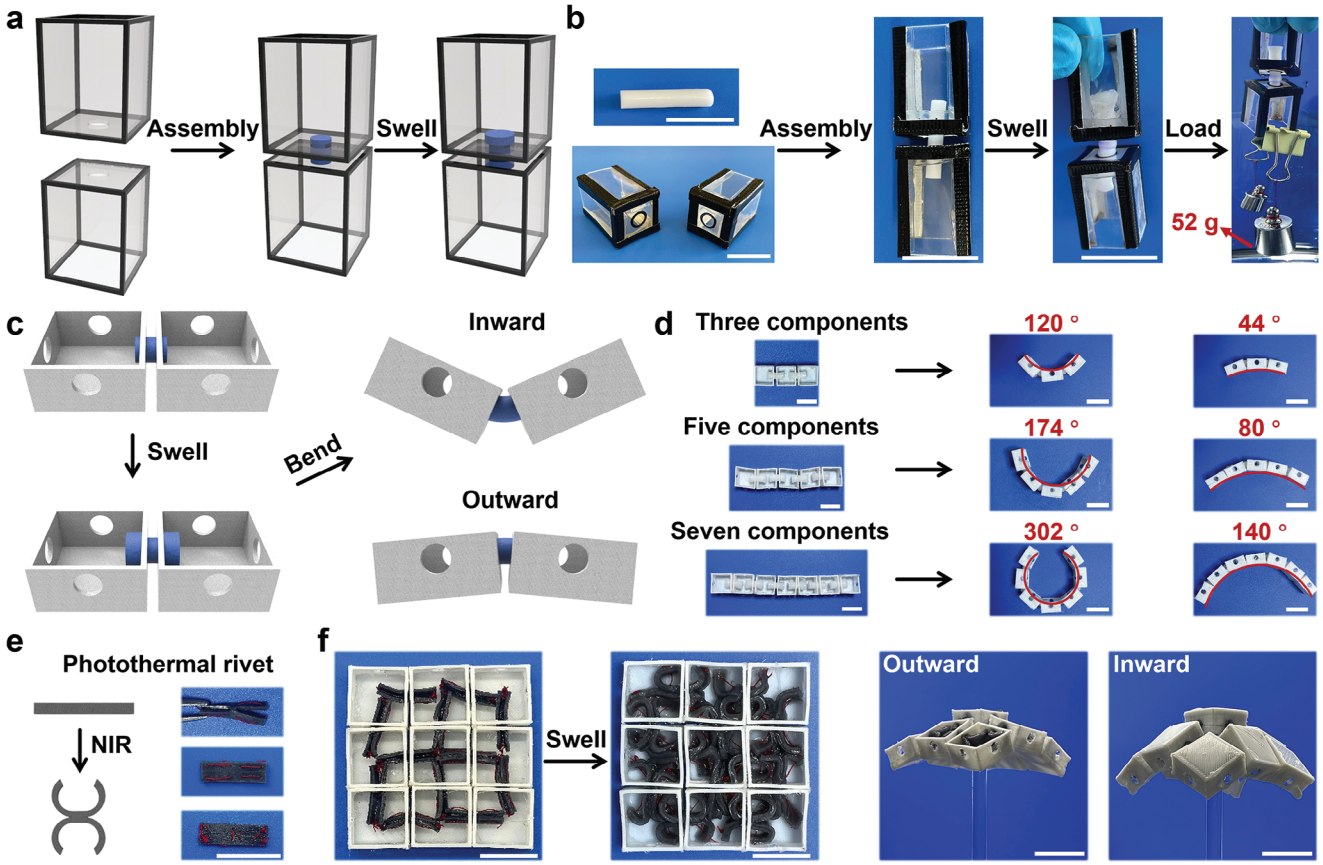

Figure 5. The demonstration of PVA-C6/P(AAm-*co*-AAc) hydrogel rivet application. a) Schematic illustration showing the process of assembling the hydrogel rivet with the components. b) Images demonstrating the assembly of hydrogel rivet and components, as well as its load-bearing capacity. c) Schematic illustration manifesting the assembly of hydrogel rivet with newly designed components. d) Images showing the series composed of different quantities of components and hydrogel rivets, and the degrees of inward and outward bending. e) PVA-C6/P(AAm-*co*-AAc) photo-thermal hydrogel rivet combining with restricting-domain method. f) Images showing a plane composed of components and PVA-C6/P(AAm-*co*-AAc) photo-thermal hydrogel rivets, and the degrees of inward and outward bending. Scale bars: 2 cm.

connection. Furthermore, through increasing contact area with water, it could experience greater swelling within a certain period, resulting in a more secure fixation of the components and increasing the load-bearing capacity (Figure S12, Supporting Information).

Based on the original components mentioned above, a new design for the components has been made by the 3D printer to enhance the versatility and application value of hydrogel rivets. As shown in Figure 5c, the PVA-C6/P(AAm-*co*-AAc) hydrogel rivet was positioned between two components, establishing a secure connection through the swelling process. Benefiting from the soft characteristics of hydrogel rivet, this soft mechanical assembly could further exhibit Janus bending performance. In detail, the varying distances between the hole and the edges of the assembly result in distinct bending characteristics. When the assembly was bent toward the edges closer to the hole (noted as inward bending), it could achieve a larger bending angle compared to bent toward the edge farther from the hole (noted as outward bending). This was because the edges of the components came into contact with each other, preventing further bending deformation. Notably, as the number of components increased to 3, 5, and 7 successively, the bending angle in inward bending rose to 302°, while in outward bending, it increased to 140°, which indicated the assembly became softer and softer (Figure 5d). Further, when more components were arranged in a 2D array, this Janus bending performance could be also replicated in a 2D flat. In this scenario, the 2D assembly exhibited robust characteristics when bending outward and soft characteristics when bending inward (Figure S13, Supporting Information).

Upon the aforementioned soft mechanical assembly, the introduction of the photo-thermal effect extends the capabilities of this assembly by enabling remote control through NIR light. This enhancement significantly broadens the scope and convenience of their potential applications. Besides, to decrease the opera time and enhance assembly strength, the restricting-domain induced deformation was incorporated. As demonstrated in Figure 5e, a PVA-C6/P(AAm-*co*-AAc) photo-thermal hydrogel sheet was folded, and a cotton cord was systematically threaded through it. Then, 4 W NIR light was irradiated onto the surface of this hydrogel, triggering the thermo-responsive swelling process and allowing it to bend toward both sides. Due to the fast light-steered assembly, such a type of hydrogel rivet was able to bear a mass that was more than 185 times its own solid content (Figure S14, Supporting Information). Similar to the PVA-C6/P(AAm-*co*-AAc)

hydrogel rivet, the PVA-C6/P(AAm-*co*-AAc) photo-thermal hydrogel rivets were also suitable for the soft mechanical assembly and exhibited Janus bending properties. When 7 rigid components were assembled, the assembly could generate a 284° bending angle inward and a 150° bending angle outward, which was similar to the result of the PVA-C6/P(AAm-*co*-AAc) hydrogel rivet (Figure S15, Supporting Information). Furthermore, when applying this approach to assemble 2D arranged components in an array, the 2D assembly effectively exhibited a softer property inward and a more robust property outward (Figure 5f). Therefore, after incorporating the restricting-domain method with photothermal effect, the time required for swelling to achieve the desired fixing effect was at least half as short as that of normal PVA-C6/P(AAm-*co*-AAc) hydrogel rivets, helping achieve the expected level of fixation more quickly and conveniently in applications.

3. Conclusion

In summary, to reconcile the inherent contradiction between achieving stable assembly and enabling soft deformations, we have proposed a universal and straightforward assembly system for soft mechanical applications. Drawing inspiration from the assembly mechanism of rivets, the PVA-C6 network was utilized as a molecular switch to continuously regulate the unidirectional swelling process of the P(AAm-*co*-AAc) network. Upon this chemical design, when the double network hydrogel was immersed in cool water, the alkyl chains (hexylamine) would aggregate due to their hydrophobicity, which functioned as the temporary cross-linker to restrict the chain's elastic-induced swelling process. Conversely, when the hydrogel was transferred into hot water, these hydrophobic clusters would quickly disassociate, releasing the restriction and restarting the swelling process. Thus, utilizing this hydrogel as a rivet, two rigid components with prefabricated hollows would be stably assembled with the swelling deformation of the ends of the hydrogel rivet. Benefiting from the inherent soft and wet properties of the hydrogel, this assembly can even generate bending deformations despite the rigid nature of the components. Furthermore, we have enhanced the deformability by incorporating knots into the hydrogel and introduced photo-thermal particles to facilitate remote controllability during the assembly process, significantly improving operability and assembly strength (the single hydrogel rivet is capable of lifting 185 times its own solid content). We believe this strategy about soft mechanical assembly may be suitable for the integration of intelligent devices and motivate the fabrication of soft robotics with multi-function integration.

Supporting Information

Supporting Information is available from the Wiley Online Library or from the author.

Acknowledgements

A.L.Y. and H.Z. contributed equally to this work. This work was supported by the National Key R&D Program of China (2022YFB3204300), Zhejiang Provincial Natural Science Foundation of China (LD22E050008), Ningbo International Cooperation Project (2023H019), and the Sino-German mobility program (M-0424).

Conflict of Interest

The authors declare no conflict of interest.

Data Availability Statement

The data that support the findings of this study are available from the corresponding author upon reasonable request.

Keywords

molecular switch, programmable deformation, shape memory, soft robot, thermo-responsive hydrogel

Received: September 30, 2023
Revised: November 11, 2023
Published online:

[1] Q. Zhang, Y. Sun, C. He, F. Shi, M. Cheng, *Adv. Sci.* **2020**, *7*, 2002025.
[2] C. Ma, T. Li, Q. Zhao, X. Yang, J. Wu, Y. Luo, T. Xie, *Adv. Mater.* **2014**, *26*, 5665.
[3] Z. Fang, H. Song, Y. Zhang, B. Jin, J. Wu, Q. Zhao, T. Xie, *Matter* **2020**, *2*, 1187.
[4] S. Zhuo, Z. Zhao, Z. Xie, Y. Hao, Y. Xu, T. Zhao, H. Li, E. M. Knubben, L. i. Wen, L. Jiang, M. Liu, *Sci. Adv.* **2020**, *6*, eaax1464.
[5] M. Cheng, G. Zhu, L. Li, S. Zhang, D. Zhang, A. J. C. Kuehne, F. Shi, *Angew. Chem., Int. Ed.* **2018**, *57*, 14106.
[6] Q. Zhao, X. Yang, C. Ma, D. Chen, H. Bai, T. Li, W. Yang, T. Xie, *Mater. Horiz.* **2016**, *3*, 422.
[7] B. Y. Wu, Y. W. Xu, X. X. Le, Y. K. Jian, W. Lu, J. W. Zhang, T. Chen, *Acta Polym. Sin.* **2019**, *50*, 496.
[8] Z. Wang, J. Xiao, T. Zhao, C. Zhang, L. Wang, N. He, Q. Kong, X. u. Wang, *Chem. Commun.* **2023**, *59*, 9818.
[9] A. Sydney Gladman, E. A. Matsumoto, R. G. Nuzzo, L. Mahadevan, J. A. Lewis, *Nat. Mater.* **2016**, *15*, 413.
[10] Y. Cheng, K. H. Chan, X.-Q. Wang, T. Ding, T. Li, X. Lu, G. W. Ho, *ACS Nano* **2019**, *13*, 13176.
[11] G. Guo, Q. Wu, F. Liu, J. Yin, Z. L. Wu, Q. Zheng, J. Qian, *Adv. Funct. Mater.* **2021**, *32*, 2108548.
[12] D. Jiao, Q. L. Zhu, C. Y. Li, Q. Zheng, Z. L. Wu, *Acc. Chem. Res.* **2022**, *55*, 1533.
[13] A. Nojoomi, J. Jeon, K. Yum, *Nat. Commun.* **2021**, *12*, 603.
[14] Y. Tan, D. i. Wang, H. Xu, Y. Yang, X.-L. Wang, F. Tian, P. Xu, W. An, X. u. Zhao, S. Xu, *ACS Appl. Mater. Interfaces* **2018**, *10*, 40125.
[15] W. Fan, C. Shan, H. Guo, J. Sang, R. Wang, R. Zheng, K. Sui, Z. Nie, *Sci. Adv.* **2019**, *5*, eaav7174.
[16] G. Ju, M. Cheng, F. Guo, Q. Zhang, F. Shi, *Angew. Chem., Int. Ed.* **2018**, *57*, 8963.
[17] C. Ma, W. Lu, X. Yang, J. He, X. Le, L. Wang, J. Zhang, M. J. Serpe, Y. Huang, T. Chen, *Adv. Funct. Mater.* **2018**, *28*, 1704568.
[18] Q. Wang, Z. Liu, C. Tang, H. Sun, L. Zhu, Z. Liu, K. e. Li, J. Yang, G. Qin, G. Sun, Q. Chen, *ACS Appl. Mater. Interfaces* **2021**, *13*, 10457.
[19] X. Ji, Z. Li, X. Liu, H.-Q. Peng, F. Song, J. Qi, J. W. Y. Lam, L. Long, J. L. Sessler, B. Z. Tang, *Adv. Mater.* **2019**, *31*, 1902365.
[20] C. Yao, Z. Liu, C. Yang, W. Wang, X.-J. Ju, R. Xie, L.-Y. Chu, *ACS Appl. Mater. Interfaces* **2016**, *8*, 21721.
[21] T. Zhao, Z. Wang, Y. Yang, K. Liu, X. u. Wang, *ACS Appl. Mater. Interfaces* **2023**, *15*, 33169.
[22] Q. Ge, Z. Chen, J. Cheng, B. Zhang, Y.-F. Zhang, H. Li, X. He, C. Yuan, J. Liu, S. Magdassi, S. Qu, *Sci. Adv.* **2021**, *7*, eaba4261.
[23] Y. Cao, G. Zhang, Y. Zhang, M. Yue, Y. Chen, S. Cai, T. Xie, X. Feng, *Adv. Funct. Mater.* **2018**, *28*, 1804604.

[24] T. Li, J. Wang, L. Zhang, J. Yang, M. Yang, D. Zhu, X. Zhou, S. Handschuh-Wang, Y. Liu, X. Zhou, *J. Mater. Chem. B* **2017**, *5*, 5726.
[25] H.-H. Park, M. Seong, K. Sun, H. Ko, S. M. Kim, H. E. Jeong, *ACS Macro Lett.* **2017**, *6*, 1325.
[26] H. Zhang, X. Guo, J. Wu, D. Fang, Y. Zhang, *Sci. Adv.* **2018**, *4*, eaar8535.
[27] W. J. Peng, J. Yin, X. M. Zhang, Y. P. Shi, G. Che, Q. Zhao, J. Liu, *Adv. Funct. Mater.* **2023**, *33*, 2214505.
[28] J. Xu, Y. Jiang, L. Gao, *J. Mater. Chem. B* **2023**, *11*, 221.
[29] B. Wu, H. Lu, X. Le, W. Lu, J. Zhang, P. Théato, T. Chen, *Chem. Sci.* **2021**, *12*, 6472.
[30] H. Hu, C. Huang, M. Galluzzi, Q. Ye, R. Xiao, X. Yu, X. Du, *Research* **2021**, *2021*, 9786128.
[31] X. Le, W. Lu, J. Zheng, D. Tong, N. Zhao, C. Ma, H. e. Xiao, J. Zhang, Y. Huang, T. Chen, *Chem. Sci.* **2016**, *7*, 6715.
[32] X. Le, W. Lu, J. Zhang, T. Chen, *Adv. Sci.* **2019**, *6*, 1801584.
[33] L. Hua, M. Xie, Y. Jian, B. Wu, C. Chen, C. Zhao, *ACS Appl. Mater. Interfaces* **2019**, *11*, 43641.
[34] Q. L. Zhu, C. Du, Y. Dai, M. Daab, M. Matejdes, J. Breu, W. Hong, Q. Zheng, Z. L. Wu, *Nat. Commun.* **2020**, *11*, 5166.
[35] S. Wang, S. Li, L. Gao, *ACS Appl. Mater. Interfaces* **2019**, *11*, 43622.
[36] C. F. Dai, X. N. Zhang, C. Du, A. Frank, H.-W. Schmidt, Q. Zheng, Z. L. Wu, *ACS Appl. Mater. Interfaces* **2020**, *12*, 53376.
[37] L. Hua, C. Zhao, X. Guan, J. Lu, J. Zhang, *Sci. China Mater.* **2022**, *65*, 2274.
[38] H. Lu, B. Wu, X. Le, W. Lu, Q. Yang, Q. Liu, J. Zhang, T. Chen, *Adv. Funct. Mater.* **2022**, *32*, 2206912.
[39] M. Xu, Y. Miao, X. Qiu, X. Song, Q. Zhao, J. Yu, L. Zhang, *ACS Appl. Mater. Interfaces* **2022**, *14*, 3591.
[40] M. T. I. Mredha, H. H. Le, J. Cui, I. Jeon, *Adv. Sci.* **2020**, *7*, 1903145.
[41] Z. J. Wang, W. Hong, Z. L. Wu, Q. Zheng, *Angew. Chem., Int. Ed.* **2017**, *56*, 15974.
[42] H. Gao, Z. Zhao, Y. Cai, J. Zhou, W. Hua, L. Chen, L. i. Wang, J. Zhang, D. Han, M. Liu, L. Jiang, *Nat. Commun.* **2017**, *8*, 15911.
[43] B. Zhang, L. Jia, J. Jiang, S. Wu, T. Xiang, S. Zhou, *ACS Appl. Mater. Interfaces* **2021**, *13*, 36574.
[44] Y. Huang, S. Qian, J. u. Zhou, W. Chen, T. Liu, S. Yang, S. Long, X. Li, *Adv. Funct. Mater.* **2023**, *33*, 2213549.
[45] Z. Xu, C. Fan, Q. Zhang, Y. Liu, C. Cui, B. o. Liu, T. Wu, X. Zhang, W. Liu, *Adv. Funct. Mater.* **2021**, *31*, 2100462.
[46] H. Lu, B. Wu, X. Yang, J. Zhang, Y. Jian, H. Yan, D. Zhang, Q. Xue, T. Chen, *Small* **2020**, *16*, 2005461.
[47] K. Liu, Y. Zhang, H. Cao, H. Liu, Y. Geng, W. Yuan, J. Zhou, Z. L. Wu, G. Shan, Y. Bao, Q. Zhao, T. Xie, P. Pan, *Adv. Mater.* **2020**, *32*, 2001693.
[48] Y. Zhang, K. Liu, T. Liu, C. Ni, D. i. Chen, J. Guo, C. Liu, J. Zhou, Z. Jia, Q. Zhao, P. Pan, T. Xie, *Nat. Commun.* **2021**, *12*, 6155.
[49] Z. Zhao, S. Zhuo, R. Fang, L. Zhang, X. Zhou, Y. Xu, J. Zhang, Z. Dong, L. Jiang, M. Liu, *Adv. Mater.* **2018**, *30*, 1804435.
[50] Z. Zhao, Y. Liu, K. Zhang, S. Zhuo, R. Fang, J. Zhang, L. Jiang, M. Liu, *Angew. Chem., Int. Ed.* **2017**, *56*, 13464.